This article was downloaded by: [King Abdullah University of Science & Technology KAUST]
On: 19 February 2015, At: 04:38
Publisher: Taylor & Francis
Informa Ltd Registered in England and Wales Registered Number: 1072954 Registered office: Mortimer House, 37-41 Mortimer Street, London W1T 3JH, UK

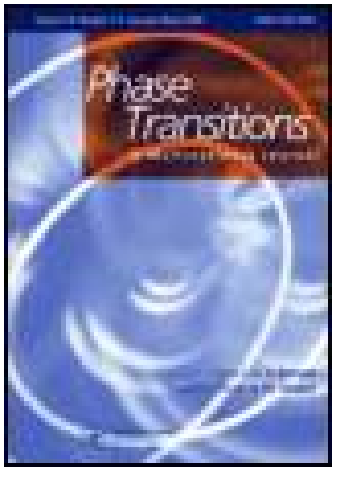

CrossMark
Click for updates

Phase Transitions: A Multinational Journal
Publication details, including instructions for authors and subscription information:
http://www.tandfonline.com/loi/gpht20

Calorimetric study of phase transitions in nanocomposites of quantum dots and a liquid crystal

P. Kalakonda[ab] & G.S. Iannacchione[a]
[a] Department of Physics, Worcester Polytechnic Institute, Worcester, MA, USA
[b] Department of Materials Science and Engineering, Carnegie Mellon University, Pittsburgh, PA, USA
Published online: 19 Feb 2015.

To cite this article: P. Kalakonda & G.S. Iannacchione (2015): Calorimetric study of phase transitions in nanocomposites of quantum dots and a liquid crystal, Phase Transitions: A Multinational Journal

To link to this article: http://dx.doi.org/10.1080/01411594.2014.1001847

PLEASE SCROLL DOWN FOR ARTICLE

Taylor & Francis makes every effort to ensure the accuracy of all the information (the "Content") contained in the publications on our platform. However, Taylor & Francis, our agents, and our licensors make no representations or warranties whatsoever as to the accuracy, completeness, or suitability for any purpose of the Content. Any opinions and views expressed in this publication are the opinions and views of the authors, and are not the views of or endorsed by Taylor & Francis. The accuracy of the Content should not be relied upon and should be independently verified with primary sources of information. Taylor and Francis shall not be liable for any losses, actions, claims, proceedings, demands, costs, expenses, damages, and other liabilities whatsoever or howsoever caused arising directly or indirectly in connection with, in relation to or arising out of the use of the Content.

This article may be used for research, teaching, and private study purposes. Any substantial or systematic reproduction, redistribution, reselling, loan, sub-licensing, systematic supply, or distribution in any form to anyone is expressly forbidden. Terms &

Conditions of access and use can be found at http://www.tandfonline.com/page/terms-and-conditions

Downloaded by [King Abdullah University of Science & Technology KAUST] at 04:38 19 February 2015

Phase Transitions, 2015
http://dx.doi.org/10.1080/01411594.2014.1001847

Taylor & Francis

Downloaded by [King Abdullah University of Science & Technology KAUST] at 04:38 19 February 2015

Calorimetric study of phase transitions in nanocomposites of quantum dots and a liquid crystal

P. Kalakonda[a,b]* and G.S. Iannacchione[a]

[a]*Department of Physics, Worcester Polytechnic Institute, Worcester, MA, USA;* [b]*Department of Materials Science and Engineering, Carnegie Mellon University, Pittsburgh, PA, USA*

(*Received 22 October 2014; accepted 16 December 2014*)

The complex specific heat is measured over a wide temperature range for the liquid crystal (LC) 4-cyano-4-octylbiphenyl (8CB) and cadmium sulfate quantum dots (QDs) composites as a function of QD concentration. The thermal scans were performed under near-equilibrium conditions for all samples having QDs weight percent (ϕ_w) from 0 to 3wt% over a wide range of temperature well above and below the two transitions in pure 8CB. Isotropic (*I*) to nematic (*N*) and nematic to smectic-*A* (Sm*A*) phase transitions evolve in character and their transition temperatures offset by (~2.3 to 2.6 K) lower for all composite samples as compared to that in pure 8CB. The enthalpy change associated with *I*–*N* phase transitions shows slightly different behavior on heating and cooling and it also shows crossover behavior at lower and higher QD content. The enthalpy change associated with *N*–Sm*A* phase transitions is independent of QD loading and thermal treatment. Given the homogeneous and random distribution of QD in these nanocomposites, we interpret that these results as arising that the nematic phase imposes self-assembly on QDs to form one-dimensional arrays leading to QDs and induces net local disordering effect in LC media.

Keywords: calorimetry; nanomaterials; liquid crystal composites; anchoring

1. Introduction

Composites of nanoparticles with complex fluids represent a unique physical system where properties of the components only partially mix and new behavior can emerge. Traditional composites are relatively well understood as the superposition, weighted by volume or mass, of the component's properties and the interfacial interactions that play a role in holding the composite together. As the quantum dots (QDs) added enough to the complex fluids, the surface area begins to dominate, leading to unique behavior of the nanocomposites. The richness of the nanocomposites that can be designed by coupling various colloids and liquid crystalline materials opens wide field of research. QDs and liquid crystals (LCs) are good examples of such components.

Controlled self-assembly of semiconductor QDs holds great promise for numerous applications, such as next-generation photonic devices, QD displays, biomedical imaging. [1–9] Recently, it has been demonstrated that nanomaterials such as nanotubes or nanorods can be organized by nematic LCs.[10–12] In this case, the anisotropic order of the LC imparts order onto the nano-size guest particles, along the nematic director average orientational direction of the LC molecules, for example, due to the reduction in excluded volume.[13] Because the director can be aligned by external electric fields, the nanoscale

*Corresponding author. Email: gsiannac@wpi.edu

© 2015 Taylor & Francis

Downloaded by [King Abdullah University of Science & Technology KAUST] at 04:38 19 February 2015

assemblies of the QDs in the LC can be manipulated. Recent research shows that a smectic LC environment allows QDs to achieve high spatial ordering into quasi-one-dimensional arrays along the director.[14] Thus, comprehensive understanding of the interaction of nanoparticles of CNT with an LC and the principles governing their self-assembly through LC mediated interactions is a very important and active area of research.

LCs [15–17] are anisotropic fluids that have numerous thermodynamically stable phases exhibiting molecular order in between an isotropic liquid and a three dimensionally ordered solid. It has been shown that to minimize elastic distortions in the LC, micrometer-size spherical particles tend to be distributed into cylindrically symmetric chain or strands along the global nematic director which is essential for minimization of excluded volume.[13] However, it is not clear how this analysis would change or remain valid as the spherical particles' diameter is reduced to nanometer scales, such as QDs. The direct first-order transition from the isotropic (*I*) to the smectic-*A* (Sm*A*) phase has attracted attention in experimental [18–26] and theoretical research [27–30] as a prototypical symmetry breaking phase transition. High-resolution synchrotron X-ray diffraction study of the *I*–Sm*A* phase transition in 10CB–aerosil showed that the transition remains first order for all gel densities with systematic evolution of correlation length.[23] The study of phase transition behavior of 10CB in the presence of silica aerogels showed that the direct *I*–Sm*A* transition occurs through the nucleation of smectic domains.[22] The effect of pressure on the *I*–Sm*A* phase transition was examined and pointed out that the effect is to increase the transition temperature and to decrease the discontinuity of the transition.[29] The macroscopic dynamic behavior was studied in the vicinity of the *I*–Sm*A* transition and the dynamic equations were presented on the *I* and Sm*A* side of the phase transition incorporating the effect of an external electric field.[30] The existence of surface-induced order was shown in the isotropic phase of 12CB, which has the direct *I*–Sm*A* transition, confined to anapore membranes through specific heat and X-ray scattering studies.[18] Recently, the research has been focused on understanding of the self-assembly, structures of various shapes of nanoparticles, and shape tuning in different LC.[31–33,34–39] All the observations showed that the *I*–Sm*A* transition is more first-order than the very weak *I*–*N* transition indicating that the orientational order of the Sm*A* phase is higher than that in the nematic phase. Even though significant effort was applied for the study of the *I*–Sm*A* transition behavior, many problems related to fundamentals of the transition are yet to be solved.

In this work, we study the phase transition behavior of the LC 4-cyano-4-octylbiphenyl (8CB) doped with cadmium sulfate QDs as a function of QD concentration. The incorporation of QDs in 8CB reveals that mesophase transition temperatures shift downward. These results suggest that the interactions between molecular structure, dipole moment of LC, and QDs can allow random dispersion of QDs to both surface and disorder effects despite being randomly dispersed and without any external field.

Our presentation is organized as follows: following this introduction, Section 2 describes the preparation of the sample and modulated differential scanning calorimetry (MDSC) procedure. Section 3 describes the calorimetric results of phase transitions in the 8CB/QD system, and Section 4 discussion and conclusions of our work and future directions.

2. Methodology

2.1. Materials and sample preparation

The LC 8CB used for this experiment was purchased from Frinton Laboratory. The 8CB has a molecular mass $M\mathrm{w} = 291.44$ g mol^{-1} and a density of $\rho_{\mathrm{LC}} = 0.996$ g ml^{-1}. Pure

Downloaded by [King Abdullah University of Science & Technology KAUST] at 04:38 19 February 2015

8CB (2.3 nm long and 0.5 nm wide molecules) has a weakly first-order isotropic (I) to nematic (N) phase transition at $T_{IN}^{0} \sim 313.98$ K, with the second-order nematic to smectic-A (SmA) transition at $T_{NA}^{0} \sim 306.97$ K. The CdS QDs (UV absorption peak: 361 nm) having a diameter of 6 nm with capping in toluene solvent dispersed were purchased from NN-Labs. Oleic acid was used as ligand and the diameter of QDs is about 6 nm. To reduce aggregation, a small amount of QDs with toluene were mixed in a vial. The 8CB was added to the toluene + QD mixture to achieve the desired final weight percent ϕ_w of QDs. The mixture was then shaken using a mixer for 30 min, followed by sonication for 3 hours to facilitate dispersion. Finally, the toluene was evaporated slowly, and then degassed under a modest vacuum in the isotropic phase of 8CB at ~364 K for about 2 hours. Microbalance massing of the mixture was done to ensure complete removal of toluene before being sealed in the experimental cells. This process was repeated to prepare 0 (pure 8CB), 0.3, 0.4, 0.5, 0.8, 1, 2, and 3wt% QD samples.

2.2. *Modulated differential scanning calorimetry*

Modulated (temperature) differential scanning calorimetry (MTDSC/MDSC) allows for the simultaneous measurement of the evolution of both the heat flow (HF) and heat capacity. It is essentially the combination of traditional ac-calorimetry with DSC. This method allows for measuring the total HF (enthalpy) as well as its non-reversible (kinetic or imaginary component) and the reversible (real component) heat capacities. A detailed description of the MDSC method can be found elsewhere.[40–46]

MDSC experiments were performed using a Model Q200 from TA Instruments, USA. Prior to all measurements, temperature calibration was done with a sapphire disc, under the same experimental conditions used for all 8CB/QD samples. The analysis method used to extract the complex specific heat is based on the linear response theory.[40] In general, a temperature oscillation is described as $T(t) = T_0 + \dot{T}_0\, t + A_{\mathrm{T}} \sin(\omega t)$, where T_0 is the initial temperature at time $t = 0$, T is the absolute temperature at time t, $\dot{T}_0$ is the baseline temperature scan rate, A_T is the temperature amplitude, and ω ($\omega = 2\pi f$) is the angular frequency of the temperature modulation. The temperature rate is also time dependent and is given by $\dot{T}(t) = dT/dt = \dot{T}_0 + A_q \cos(\omega t)$, where A_q is the amplitude of the temperature modulation rate ($Aq = \omega AT$). Since the applied temperature rate consists of two components, $\dot{T}_0$ the underlying rate and $A_q \cos(\omega t)$ the periodic rate, the measured HF also can be separated into two components in response to these rates. The periodic component can be described by $H_{\mathrm{FQ}} = A_{\mathrm{HF}} \cos(\omega \mathrm{t} - \phi)$, where A_{HF} is the amplitude of the HF and ϕ is the phase angle between HF and temperature rate. The absolute value of the complex specific heat is written as $C_p^* = A_{\mathrm{HF}}/mA_{\mathrm{Q}}$ where m is the mass of the sample. The phase angle ϕ requires a small correction (calibration) to account for finite thermal conductivities of the sample and cell. See [46].

The real (reversible) C_p' and imaginary (non-reversible) C_p'' parts of the specific heat are then given by

$$C_p' = C_p^* \mathrm{Cos}(\phi), \tag{1}$$

$$C_p'' = C_p^* \mathrm{Sin}(\phi), \tag{2}$$

which allow for a consistent definition of the complex specific heat. Typically, under equilibrium conditions, $C_p'' = 0$, after ϕ correction (or have a weak linear temperature dependence remaining). The appearance of a peak-like non-zero C_p'' feature

Downloaded by [King Abdullah University of Science & Technology KAUST] at 04:38 19 February 2015

commensurate with a peak in the real part of the specific heat indicates that this feature arises from a first-order transition and involves a latent heat, where the total heat capacity is given by $C = \sqrt{Cp'^2 + Cp''^2}$. The excess specific heats were determined in order to isolate the contribution from the various transitions. A linear baseline was used over the entire temperature scan range in order to determine $\Delta C_p = C_p - C_{\text{baseline}}$ for both the real and imaginary components, though always exhibited a very shallow linear baseline that was very close to zero, indicating near-equilibrium conditions for the experimental parameters used in this work. For specific heat features that are close together in temperature, the wing of one peak (usually the higher temperature peak) is subtracted from the lower specific heat peak in order to isolate the excess specific heat of the lower temperature transition, denoted as $\delta C_p = \Delta C_p - C_{\text{wing}}$, where for C_{wing} we used a mimic function (polynomial) for the underlying wing. This calculation was applied only to the real component of the specific heat. Figure 1 illustrates this subtraction; the dashed-dot line represents the background.

The particular transition enthalpy component is simply the integration of the excess specific heat component over a consistent temperature range, e.g. $\Delta H = \Delta C_p' \, dT$ for the real and $\Delta H = \Delta C_p'' \, dT$ for the imaginary enthalpy. The total magnitude of the transition enthalpy is defined as $\Delta H = \sqrt{(\Delta H')^2 + (\Delta H'')^2}$. Finally, for the first-order transition, the transition temperature (T_{IN}) is determined as the highest temperature of the two-phase

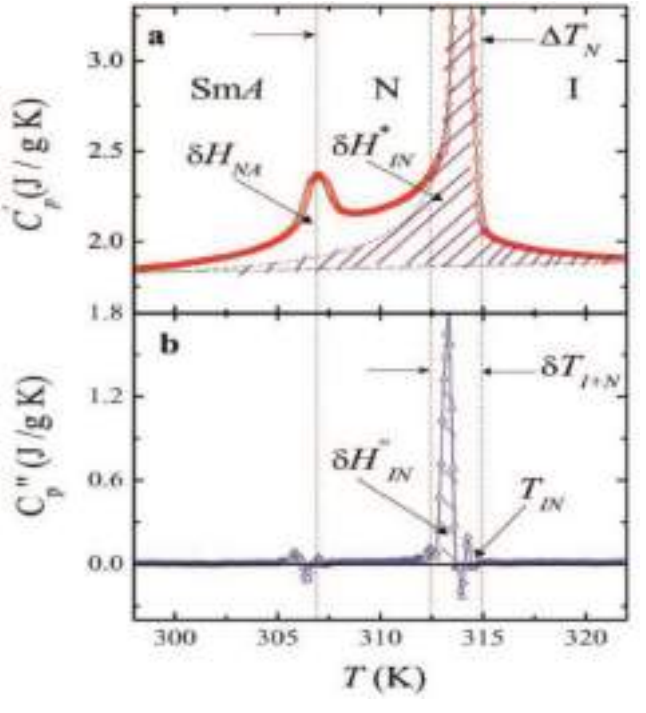

Figure 1. (a) Real part of specific heat C_p as a function of temperature on heating for 8CB sample. The dashed line represents a wing subtraction and dashed-dot line represents base line subtraction. (b) Imaginary part of specific heat ΔC_p as a function of temperature on heating for 8CB sample.

Downloaded by [King Abdullah University of Science & Technology KAUST] at 04:38 19 February 2015

coexistence region indicated by the onset of non-zero values of $\Delta C_p''$. For continuous transition, the transition temperature is taken as the peak temperatures $\Delta C_p'$. The nematic range is defined as $\Delta T_N = T_{IN} - T_{NA}$ and the co-existence region ΔT_{I+N}, is determined taking the difference of high-temperature and low-temperature limits of peak C_p''. Quasi-equilibrium parameters such as scan rate, temperature amplitude, and modulation time period were determined varying their values until rate effects were minimized. However, the final parameters only approximate equilibrium conditions.

3. Results

3.1. Overview

For pure 8CB, from the same batch used for all mixture samples, the $I-N$ phase transition occurs at $T_{IN} = 313.91$ K while the $N-\mathrm{Sm}A$ transition occurs at $T_{NA} = 307$ K, agreeing well with the values reported in the literature.[47] In addition, the effective enthalpy $\Delta H_{IN}^{*} = 6.05 \pm 0.15$ J/g, the dispersive enthalpy $\Delta H_{IN}'' = 1.33 \pm 0.05$ J/g, and the effective enthalpy $\delta H_{NA}^{*} = 0.68 \pm 0.03$ J/g in pure 8CB, which is within 8% of the literature value.[48] These results indicate the relative purity of the LC and used for comparison to the LC/QD composite results. A summary of transition temperatures, the nematic temperature ranges, and enthalpies for all samples on cooling and heating are given in Tables 1 and 2.

For the $I-N$ phase transition, an expanded view of the $I-N$ excess specific heat $\Delta C_p'$ on cooling and heating are shown in Figure 2 over a temperature range 7 K about T_{IN}. Here, ΔC_p are presented in J/K/g of the sample. The $\Delta C_p'$ peak height for cooling and heating scans within the two-phase $I+N$ coexistence region is rising up to $\phi_w \sim$ 0.3wt%, and then it decreases with further increasing $\phi_w \sim$ 3wt%. The hysteresis in $\Delta C_p'$ is also observed in the two-phase region $I+N$ between heating and cooling with the heating $\Delta C_p'$ peaks are slightly higher in temperature for above $\phi_w > 0.65$wt% composite samples. The $\Delta C_p'$ peaks for $I-N$ phase transition in 8CB/QD composite samples at higher QD loading are slightly broader. The $\Delta C_p'$ and $\Delta C_p''$ behavior are consistent on heating and cooling, as well as being reproducible after multiple thermal cycles. The

Table 1. Summary of the calorimetric results for pure and all 8CB/QD samples on cooling. Shown are quantum dots weight percent φ_w, the $I-N$ transition temperature T_{IN}, the $N-\mathrm{Sm}A$ transition temperature T_{NA}, the nematic range ΔT_{TN}, the coexistence range ΔT_{I+N}, the integrated enthalpy change ΔH_{IN}^{*}, the imaginary enthalpy $\Delta H_{IN}''$, and the integrated enthalpy for $N-\mathrm{Sm}A$ transition ΔH_{NA}^{*}. All temperatures are in K and enthalpies are in J/g. The heating and cooling scan rate 0.5 K/min has been used.

φ_w (wt.%)	T_{IN}	T_{NA}	ΔT_N	ΔT_{I+N}	ΔH_{IN}^{*}	$\Delta H_{IN}''$	ΔH_{NA}^{*}
0.0	313.91 ± 0.16	307.00 ± 0.15	6.91 ± 0.13	1.71 ± 0.04	6.05 ± 0.15	1.33 ± 0.15	0.68 ± 0.07
0.3	313.72 ± 0.20	306.57 ± 0.24	7.01 ± 0.12	1.75 ± 0.05	5.31 ± 0.20	1.35 ± 0.20	0.76 ± 0.06
0.4	313.52 ± 0.25	306.65 ± 0.25	6.87 ± 0.11	1.77 ± 0.03	5.36 ± 0.20	1.38 ± 0.15	0.75 ± 0.07
0.5	313.50 ± 0.15	306.61 ± 0.23	6.89 ± 0.13	1.76 ± 0.04	5.65 ± 0.30	1.36 ± 0.13	0.75 ± 0.08
0.8	313.35 ± 0.20	306.52 ± 0.20	6.83 ± 0.12	1.73 ± 0.03	5.92 ± 0.30	1.38 ± 0.15	0.81 ± 0.06
1.0	313.02 ± 0.21	306.33 ± 0.23	6.69 ± 0.13	1.74 ± 0.05	5.97 ± 0.10	1.36 ± 0.14	0.78 ± 0.07
2.0	312.61 ± 0.13	305.69 ± 0.24	6.70 ± 0.12	1.86 ± 0.02	5.84 ± 0.20	1.40 ± 0.20	0.78 ± 0.08
3.0	310.83 ± 0.11	304.46 ± 0.22	6.37 ± 0.11	2.22 ± 0.03	5.61 ± 0.25	1.37 ± 0.14	0.86 ± 0.07

Downloaded by [King Abdullah University of Science & Technology KAUST] at 04:38 19 February 2015

Table 2. Summary of the calorimetric results for pure and all 8CB/QD samples on heating. Shown are quantum dots weight percent ϕ_w, the $I-N$ transition temperature T_{IN}, the $N-$SmA transition temperature T_{NA}, the nematic range ΔT_{TN}, the coexistence range ΔT_{I+N}, the integrated enthalpy change ΔH^*_{IN}, the imaginary enthalpy $\Delta H''_{IN}$, and the integrated enthalpy for $N-$SmA transition ΔH^*_{NA}. All temperatures are in K and enthalpies are in J/g. The heating and cooling scan rate 0.5 K/min has been used.

φ_w (wt.%)	T_{IN}	T_{NA}	ΔT_N	ΔT_{I+N}	ΔH^*_{IN}	$\Delta H''_{IN}$	ΔH^*_{NA}
0.0	313.90 ± 0.165	306.95 ± 0.13	6.95 ± 0.11	1.64 ± 0.05	6.07 ± 0.31	1.33 ± 0.15	0.72 ± 0.06
0.3	313.70 ± 0.24	306.78 ± 0.24	7.01 ± 0.13	1.56 ± 0.05	6.48 ± 0.20	1.31 ± 0.20	0.73 ± 0.07
0.4	313.73 ± 0.25	306.55 ± 0.25	7.18 ± 0.12	1.61 ± 0.04	6.60 ± 0.30	1.32 ± 0.14	0.72 ± 0.06
0.5	313.63 ± 0.23	306.58 ± 0.22	7.23 ± 0.13	1.57 ± 0.05	6.51 ± 0.35	1.35 ± 0.13	0.73 ± 0.07
0.8	313.81 ± 0.20	306.58 ± 0.24	7.23 ± 0.13	1.67 ± 0.04	6.48 ± 0.20	1.34 ± 0.14	0.71 ± 0.08
1.0	313.37 ± 0.23	306.42 ± 0.23	6.90 ± 0.11	1.54 ± 0.05	5.31 ± 0.25	1.33 ± 0.15	0.75 ± 0.07
2.0	313.00 ± 0.24	306.15 ± 0.22	6.85 ± 0.12	1.72 ± 0.04	5.30 ± 0.30	1.34 ± 0.16	0.71 ± 0.06
3.0	310.23 ± 0.23	304.60 ± 0.23	6.63 ± 0.13	1.92 ± 0.07	5.01 ± 0.28	1.29 ± 0.15	0.71 ± 0.07

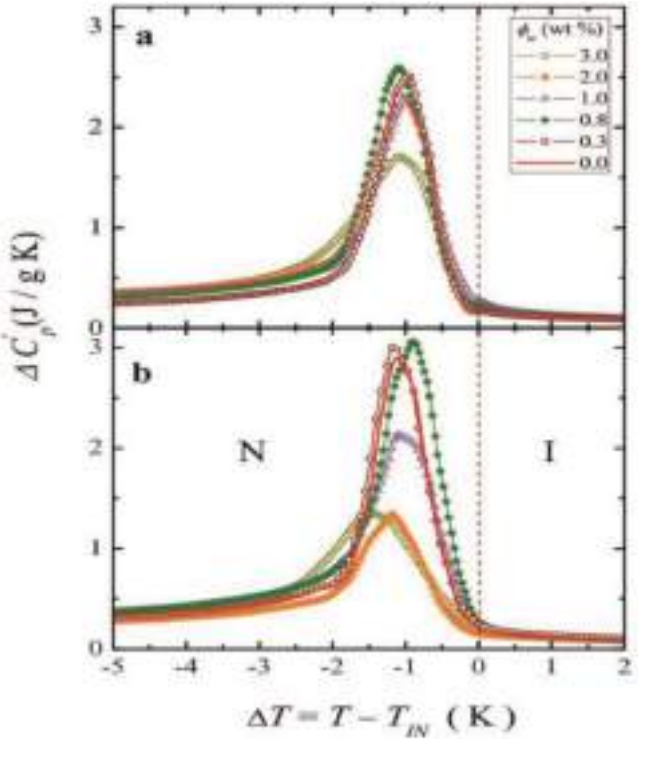

Figure 2. Excess real specific heat ΔC_p associated with the $I-N$ phase transition as function of temperature about T_{IN} on cooling (a) and heating (b). The definition of the symbols are given in the inset.

Downloaded by [King Abdullah University of Science & Technology KAUST] at 04:38 19 February 2015

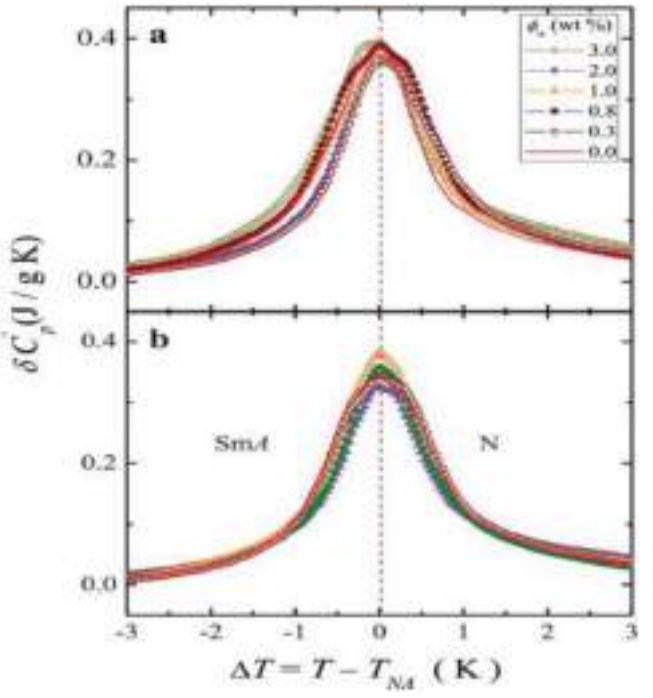

Figure 3. (a) Excess real specific heat δC_p associated with the $N-\mathrm{Sm}A$ phase transition as function of temperature about T_{NA} on cooling. The definition of the symbols are given in the inset. (b) Excess real specific heat δC_p associated with the $N-\mathrm{Sm}A$ phase transition as function of temperature about T_{NA} on heating.

$\Delta C_p'$ wings above and below *I*--*N* transition matches each other that of pure 8CB and 8CB/QD composite samples on heating and cooling. The consistency of $\Delta C_p'$ data on heating and cooling show that the sample does not phase separate on the macroscopic level. However, the microscopic (nanoscopic) phase separation and diffusion of QD into LC media may still form different configuration in *N* and $N-\mathrm{Sm}A$ phases for higher QD concentration.

For the $N-\mathrm{Sm}A$ phase transition, the excess specific heat $\delta C_p'$ vs. temperature about T_{NA} on cooling and heating as a function of temperature is shown in Figure 3 for pure 8CB and 8CB/QD composite samples. For all samples, the $N-\mathrm{Sm}A$ phase transition does not exhibit any feature in the imaginary specific heat, indicating an apparent absence of latent heat and a likely continuous transition. The $\delta C_p'$ of $N-\mathrm{Sm}A$ phase transition shows a lower wing on the Sm*A* side for 8CB/QD composite samples compared to pure 8CB. The $\delta C_p'$ of the $N-\mathrm{Sm}A$ transition of all composite samples overlay each other for all ϕ_w and pure 8CB on the Sm*A* side where they are systematically above that of pure 8CB on the nematic side of the transition. Given no strong change in the $\delta C_p'$ behavior as a function of ϕ_w, no power law fits were attempted.

3.2. *Phase diagram*

The $I-N$ and $N-\mathrm{Sm}A$ phase transition temperature as the function of ϕ_w are shown in Figure 4 on heating and cooling scans. The $I-N$ phase transition temperature T_{IN} is defined as the temperature of C_p inflection point on the high-temperature side of the C_p

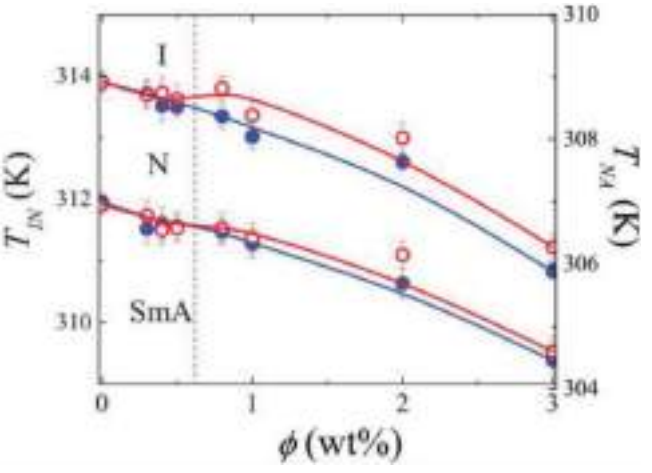

Figure 4. The $I-N$ phase transition temperatures T_{IN} [left axis: heating (○) and cooling (●)] and $I-$SmA phase transition temperature T_{NA} [right axis: heating (○) and cooling (●)] as a function of φ_w. Lines are guides for the eye.

peak.[48] Here, T_{IN} represents the lowest stable temperature of the isotropic phase. The N--SmA phase transition temperature T_{NA} is taken as C_p peak temperature. The T_{IN} and T_{NA} suppresses 2.67 and 2.35 K, respectively, with loading of QDs. Because of the uncertainty in the homogeneity of the 8CB/QD composite samples, the small noise appeared in the transition temperatures can be related to perfect mixing of 8CB/QD samples. The nematic temperature range, ΔT_N slightly increases on heating up to 0.65wt% QDs then decreases by 0.5 K with increasing ϕ_w as shown in Figure 5 (a) and the nematic range ΔT_N decreases on cooling with increasing ϕ_w. The ΔT_{I+N} coexistence region is constant up to 0.65wt% QDs loading and then increases with higher loading of QDs on heating and cooling as shown in Figure 5 (b). The $\Delta T_{I\ +N}$ increases 1 K on cooling and 0.5 K on heating as the function of QDs loading. For concentration $\phi_w \leq$.65wt%, $I-N$ and N--SmA move together and no change in coexistence range, for $\phi_w \geq$ 0.65wt%, $I-N$ transition temperature decreases faster than $N-$SmA phase and coexistence region widens with increasing ϕ_w.

3.3. *The* I−N *and* N−*Sm*A *phase transition enthalpy*

The effective $I-N$ transition enthalpy δH_T^* was obtained by integrating ΔC_p from 290 to 330 K for pure 8CB and 8CB/QD composite samples then subtracting the $N-$SmA transition enthalpy. See Figure 1.

The resulting δH_{IN}^* and $\delta H_{IN}''$ for the heating and cooling scans as the function of ϕ_w for pure 8CB and 8CB/QD composite samples are shown in Figure 6 (a). The $N-$SmA transition enthalpy for heating and cooling as the function of pure 8CB and 8CB/QD composite samples are shown in Figure 6(b). The transition enthalpies δH_{IN}^* of the $I-N$ phase for 8CB/QD composite samples show crossover behavior on heating and cooling at 0.65wt% QDs loading. There is a slight hysteresis observed between cooling and heating. The imaginary part of enthalpy $\delta H_{IN}''$ on heating and cooling is constant within the experimental uncertainties as the function of ϕ_w, which indicates latent heat is constant as the function of ϕ_w as shown in Figure 6(a). The transition enthalpy of $N-$SmA phase

Downloaded by [King Abdullah University of Science & Technology KAUST] at 04:38 19 February 2015

Downloaded by [King Abdullah University of Science & Technology KAUST] at 04:38 19 February 2015

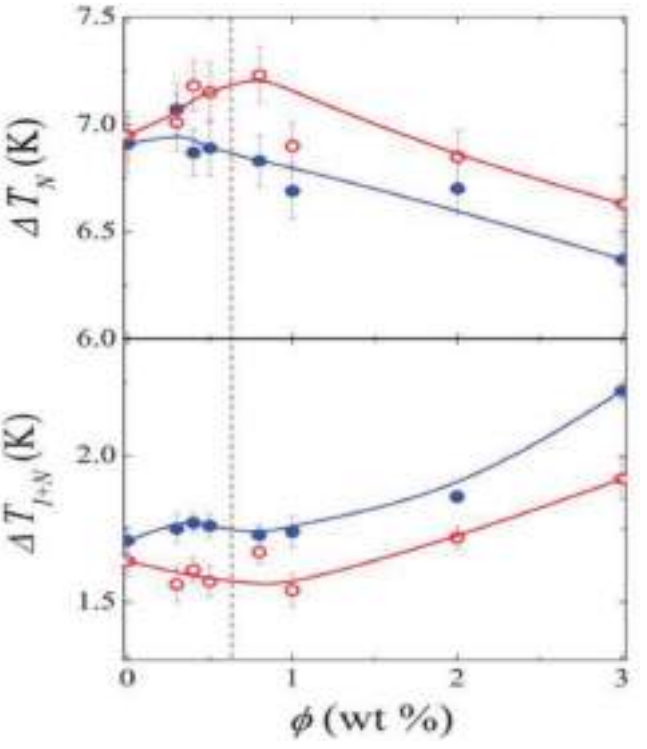

Figure 5. (a) The nematic range on heating (○) and cooling (●) as a function of ϕ_w. (b) The $I+N$ coexistence region on heating (○) and cooling (●) as a function of ϕ_w. Lines are guides for the eye.

transition δH^*_{NA} is also constant within the experimental uncertainties as the function of ϕ_w, which means smectic fluctuations remain constant as shown in Figure 6(b).

4. *Discussion and conclusions*

Suspending colloidal particles in LCs can be carried out with the aim of making new materials which exhibit new physical properties. In this section, we briefly review some of recent work done on colloidal self-assemblies in LCs and connect our work with recent studies. Using three-dimensional numerical modeling, the self-assembly of triangular, square and pentagonal sub-micrometer sized platelets was studied in a thin layer of nematic LC.[32] The inter-particle potential depends in a complex way on the orientation of the particle and the particles form linear chains at higher concentration to minimize their free energy. A theory has not yet developed to study such nano-size particles and the behavior of nanoparticle interactions depends on the nature of the LC, the anchoring conditions and the particle size. Exploring the re-orientations and interactions potential between nano-sized particles will be interesting in nanoscale photonics applications. In this study, we proposed a physical model to explain experimental results as shown in Figure 7.

The key observations of the $I-N$ C_p peak change with loading of QDs whereas the $N-$SmA phase C_p peak remains the same. There is a crossover behavior observed at 0.65wt% QD loading and for $\phi_w \geq$ 0.65wt% QD loading, all transition temperatures decrease with increasing ϕ_w. Since only ϕ_w changes, these effects may be coming from

Downloaded by [King Abdullah University of Science & Technology KAUST] at 04:38 19 February 2015

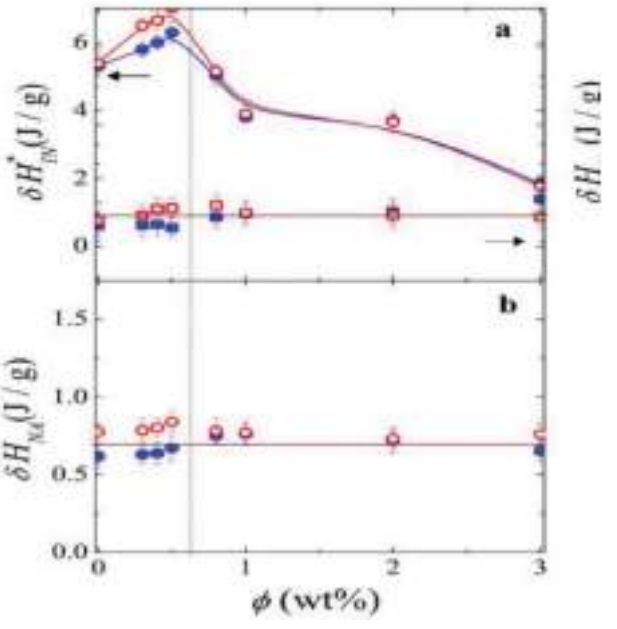

Figure 6. (a) The integrated ΔC_p I–N enthalpy δH^* [left axis: heating (○) and cooling (●)] and imaginary enthalpy δH [right axis: heating (○ and cooling (●)] as the function of ϕ_w. (b) The integrated δC_p N–SmA enthalpy δH^* on heating (○) and cooling (●) as the function of ϕ_w. Lines are guides for the eye.

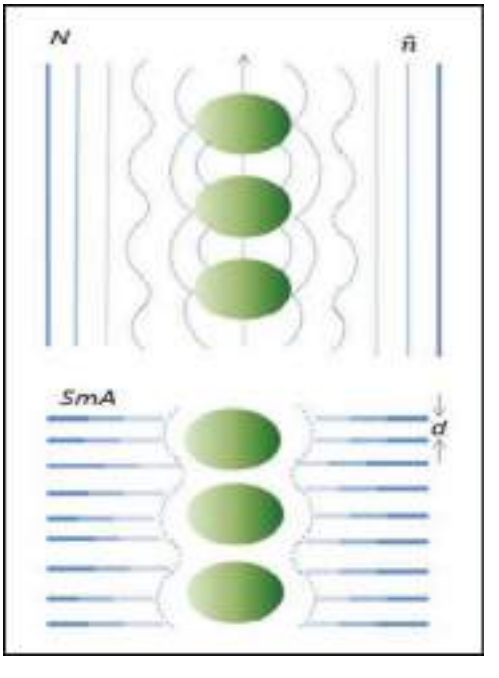

Figure 7. The QD configuration in LC media at higher QD concentration in N phase (top panel) and the QD configuration in LC media at higher QD concentration in SmA phase (bottom panel).

Downloaded by [King Abdullah University of Science & Technology KAUST] at 04:38 19 February 2015

QD arrangements below and above 0.65wt% loading. The arrangement of QDs may be different in both *N* and Sm*A* phases. Considering the spherical symmetry of the QDs, for the dilute regime, the QDs are likely to be independent (dilute ideal gas). For higher loading of ϕ_w, QDs are more likely to form groups. The free energy is minimum when dealing with spherical particles in uniaxial phase and forms a 'pearl-necklace' chain of QDs. This arrangement more closely matched the symmetry of the nematic phase. This effect is essentially independent of surface anchoring of the director $\hat{n}$, but it is most likely radial. However Sm*A* is not coupled. In the cooling process, the system moves from disorder state to order state, QDs form highly anisotropic structures along nematic director and nematic range is decreased for $\phi_w \geq 0.65$wt%. In Sm*A* phase, the size of QDs is much larger than the nematic layer and QDs do not pin the molecule. As a result, the Sm*A* phase remains bulk-like. On heating, the Sm*A*−*N* and *N*−*I* phase transition temperatures are higher than cooling transition temperatures and the *I*−*N* phase transition temperatures decrease faster than for the *N*−Sm*A* phase. This leads to the two-phase coexistence range increases for $\phi_w \geq 0.65$wt%. The QDs form a 'pearl-necklace' chain configuration for $\phi_w \geq 0.65$wt% due to minimization of their free energy as shown in the top panel of Figure 7. The effect of QDs on Sm*A* phase remains same due to the size of QDs larger than the nematic layer shown in the bottom panel of Figure 7. This leads to the effective transition enthalpy for *N*−Sm*A* phase remaining bulk-like in its behavior. On cooling at low ϕ_w, the *N* nucleates in between QDs and hence coexistence range shifts to minimum free energy state. At higher ϕ_w, QDs do not move away due to the pinning of QDs as chains and as a result enthalpy δH becomes stabilized. On heating, at lower loading of QDs, the *N* phase remains at minimum free energy state with QDs' stable positions and hence the melting process behaves as bulk-like. At higher ϕ_w, QD chains stabilize the *N* phase to para-nematic phase and hence the transition enthalpy reduces to *I* phase. As a result, the nematic phase imposes self-assembly on QDs to form one-dimensional arrays leading to QDs and induces net local disordering effect in LC media.

We have presented a detailed calorimetric study on the effect of sphere-like particles with QDs on phase transitions of the 8CB/QD nanocomposites as a function of QD loading. The complex specific heat was measured over a wide range of temperature for 8CB/QD composites as a function of QD concentration. The thermal scans were performed under near-equilibrium conditions between 290 and 330 K, first cooling followed by heating scans, for concentration of QDs ϕ_w ranging from 0 to 3wt%. The *I*−*N* phase transition temperature 2.67 K and *N*−Sm*A* phase transition temperature 2.35 K suppress for composite samples compared to the pure 8CB. The enthalpy change associated with *I*−*N* phase transitions shows slightly differently on heating and cooling and it also shows crossover behavior at lower and higher QD content. The enthalpy change associated with *N*−Sm*A* phase transitions is independent of the QD concentration and thermal treatment. The order of the transition remains the same, with the *I*−*N* weakly first-order and the *N*−Sm*A* second-order. The behavior of QDs depends sensitively on the nature of the LC, the anchoring conditions and the QD size. The results clearly demonstrate that the nematic phase imposes self-assembly on QDs to form one-dimensional arrays leading to QDs and induces net local disordering effect in LC media. Continued experimental efforts probing the homogeneity of the sample, frequency-dependent dynamics and elastic behavior via light scattering of the homogeneous sample as a function of CNT concentration and temperature would be particularly important and interesting in photonic applications.

Acknowledgments

This work was supported by the Department of Physics at WPI and a grant from the NSF award [DMR-0821292(MRI)].

Downloaded by [King Abdullah University of Science & Technology KAUST] at 04:38 19 February 2015

Disclosure statement

No potential conflict of interest was reported by the authors.

References

[1] Tong X, Zhao Y. Liquid-crystal gel-dispersed quantum dots: reversible modulation of photoluminescence intensity using an electric field. J Am Chem Soc. 2007;129:6372–6373.

[2] Lee SW, Mao C, Flynn CE, Belcher AE. Ordering of quantum dots using genetically engineered viruses. Science. 2002;296:892–895.

[3] Jiang C, Xu S, Yang D, Zhang F, Wang W. Synthesis of glutathione-capped CdS quantum dots and preliminary studies on protein detection and cell fluorescence image. Luminescence. 2007;22(5):430–437.

[4] Zhao J, Bardecker JA, Munro AM, Liu MS, Niu Y, Ding IK, Ginger DS. Efficient CdSe/CdS quantum dot light-emitting diodes using a thermally polymerized hole transport layer. Nano Lett. 2006;6(3):463–467.

[5] Balandin A, Wang KL, Kouklin N, Bandyopadhyay S. Raman spectroscopy of electrochemically self-assembled CdS quantum dots. Appl Phys Lett. 2000;76(2):137–139.

[6] Wang KL, Balandin A. Quantum dots: properties and applications. In: Markel VA, George TF, editors. *Optics of nanostructured materials*. New York (NY): Wiley; 2000.

[7] Fafard S, Wasilewski ZR, Allen CN, Picard D, Piva PG, McCaffrey JP, Molecular beam epitaxy of THz quantum cascade lasers. Superlattices Microstruct. 1999;25:87–96.

[8] Chen W, Chen W, Joly AG, Malm JO, Bovin JO, Wang S. Full-color emission and temperature dependence of the luminescence in poly-P-phenylene ethynylene-ZnS/Mn2+ composite particles. J Phys Chem B. 2003;107(27):6544–6551.

[9] Tamborra M, Striccoli M, Comparelli R, Curri ML, Petrella A, Agostiano A. Optical properties of hybrid composites based on highly luminescent CdS nanocrystals in polymer. Nanotechnology. 2004;15(4):S240–S244.

[10] Dierking I, Scalia G, Morales P. Liquid crystal–carbon nanotube dispersions. J Appl Phys. 2005;97(4):044309.

[11] Lynch MD, Patrick DL. Organizing carbon nanotubes with liquid crystals. Nano Lett. 2002;2 (11):1197–1201.

[12] Kalakonda P, Basu R, Nemitz IR, Rosenblatt C, Iannacchione GS. Studies of nanocomposites of carbon nanotubes and a negative dielectric anisotropy liquid crystal. J Chem Phys. 2014;140(10):104908.

[13] Basu R, Iannacchione GS. Carbon nanotube dispersed liquid crystal: a nano electromechanical system. Appl Phys Lett. 2008;93(18):183105.

[14] Onsager L. The effects of shape on the interaction of colloidal particles. Ann N Y Acad Sci. 1999;51:627–659.

[15] de Gennes PG, Prost J. The physics of liquid crystals. Clarendon: Oxford University Press; 1993.

[16] Chandrashekhar S. Liquid crystals. England: Cambridge University Press; 1992.

[17] Kalakonda P, Kashuri H, Kashuri K, Iannacchione GS. Calorimetric and dielectric study of a negative dielectric anisotropy alkoxy-phenyl-benzoate liquid crystal. Indian J Pure Appl Phys. 2014;52(10):689–698.

[18] Iannacchione GS, Mang JT, Kumar S, Finotello D. Surface-induced discrete smectic order in the isotropic phase of 12CB in cylindrical pores. Phys Rev Lett. 1994;73(20):2708–2711.

[19] Olbrich M, Brand HR, Finkelmann H, Kawasaki K. Fluctuations above the smectic-A-isotropic transition in liquid crystalline elastomers under external stress. Europhys Lett. 1995;31 (5–6):281–286.

[20] Bellini T, Rappaport AG, Clark NA, Thomas BN. First-order transitions and hexatic ordering in the aerogel-confined liquid crystal 650BC. Phys Rev Lett. 1996;77(12):2507–2510.

[21] Drozd-Rzoska A, Rzoska SJ, Ziołо J. Quasicritical behavior of dielectric permittivity in the isotropic phase of smectogenic n-cyanobiphenyls. Phys Rev E. 2000;61(5):5349–5354.

[22] Bellini T, Clark NA, Link DR. Isotropic to smectic A phase transitions in a porous matrix: a case of multiporous phase coexistence. J Phys Condensed Matter. 2003;15(1):S175.

[23] Ramazanoglu MK, Clegg PS, Birgeneau RJ, Garland CW, Neubert ME, Kim JM. First-order isotropic–smectic-a transition in liquid-crystal–aerosil gels. Phys Rev E. 2004;69(6):061706.

[24] Leys J, Sinha G, Glorieux C, Thoen J. Influence of nanosized confinements on 4-n-decyl-4′-cyanobiphenyl (10CB): a broadband dielectric study. Phys Rev E. 2005;71(5):051709.

Downloaded by [King Abdullah University of Science & Technology KAUST] at 04:38 19 February 2015

[25] Kędziora P. Short-range order fluctuation in the isotropic phase of solutions of 4-trans-4'-n-dodecylcyanobiphenyl in benzene studied by nonlinear dielectric spectroscopy. Acta Physica Polonica A. 2005;107(6):907–916.
[26] Chahine G, Kityk A, Knorr K, Lefort R, Guendouz M, Morineau D, Huber P. Criticality of an isotropic-to-smectic transition induced by anisotropic quenched disorder. Phys Rev E. 2010;81(3):031703
[27] Lelidis I, Durand G. Landau model of electric field induced smectic phases in thermotropic liquid crystals. J de Physique Arch. 1996;6(10):1359–1387.
[28] Mukherjee PK, Pleiner H, Brand HR. Simple Landau model of the smectic-A-isotropic phase transition. Euro Phys J E. 2001;4(3):293–297.
[29] Mukherjee PK. Effect of nonmesogenic solute on the nematic-smectic-A phase transition. J Chem Phys. 2002;116(21):9531–9536.
[30] Mukherjee PK, Rzoska SJ. Pressure effect on the smectic-A–isotropic phase transition. Phys Rev E. 2002;65(5):051705.
[31] Senyuk B, Evans JS, Ackerman PJ, Lee T, Manna P, Vigderman L, Smalyukh II. Shape-dependent oriented trapping and scaffolding of plasmonic nanoparticles by topological defects for self-assembly of colloidal dimers in liquid crystals. Nano Lett. 2012;12(2):955–963.
[32] Dontabhaktuni J, Ravnik M, Zumer S. Shape-tuning the colloidal assemblies in nematic liquid crystals. Soft Matter. 2012;8:1657–1663.
[33] Jeong J, Kim MW. Confinement-induced transition of topological defects in smectic liquid crystals: from a point to a line and pearls. Phys Rev Lett. 2012;108(20):207802.
[34] Verma R, Dhar R, Agrawal VK, Rath MC, Sarkar SK, Wadhawan VK, Dabrowski R. Electron beam irradiation-induced transformations in the electrical properties of 4'-octyl-4-cyanobiphenyl (8CB). Liquid Crystals. 2009;36(9):1003–1014.
[35] Supreet KS, Raina KK, Pratibha R. Enhanced stability of the columnar matrix in a discotic liquid crystal by insertion of ZnO nanoparticles. Liquid Cryst. 2014;40(2):228–236.
[36] Mishra M, Kumar S, Dhar R. Effect of dispersed colloidal gold nanoparticles on the electrical properties of a columnar discotic liquid crystal. RSC Adv. 2014;4(107):62404–62412.
[37] Urbanski M, Mirzaei J, Hegmann T, Kitzerow HS. Nanoparticle doping in nematic liquid crystals: distinction between surface and bulk effects by numerical simulations. Chem Phys Chem. 2014;15(7):1395–1404.
[38] Hsu CJ, Kuo CC, Hsieh CD, Huang CY. Effects of silica nanoparticles on electro-optical properties of polymer-stabilized liquid crystals. Opt Express. 2014;22(15):18513–18518.
[39] Basu R., Garvey A. Effects of ferroelectric nanoparticles on ion transport in a liquid crystal. Appl Phys Lett. 2014;105(15):151905.
[40] Schawe JEK. Principles for the interpretation of modulated temperature DSC measurements. Part 1. Glass transition. Thermochimica Acta. 1995;261:183–194.
[41] Coleman NJ, Craig DQ. Modulated temperature differential scanning calorimetry: a novel approach to pharmaceutical thermal analysis. Int J Pharmaceutics. 1996;135(1):13–29.
[42] Hutchinson JM, Montserrat S. The application of modulated differential scanning calorimetry to the glass transition. J Thermal Anal Calorimetry. 1996;47(1):103–115.
[43] Hensel A, Dobbertin J, Schawe JEK, Boller A, Schick C. Temperature modulated calorimetry and dielectric spectroscopy in the glass transition region of polymers. J Thermal Anal Calorimetry. 1996;46(3):935–954.
[44] Wunderlich B. Modeling the heat flow and heat capacity of modulated differential scanning calorimetry. J Thermal Anal Calorimetry. 1997;48(2):207–224.
[45] Aubuchon SR, Gill PS. The utility of phase correction in modulated DSC. J Thermal Anal Calorimetry. 1997;49(2):1039–1044.
[46] Weyer S, Hensel A, Schick C. Phase angle correction for TMDSC in the glass-transition region. Thermochimica Acta. 1997;304:267–275.
[47] Zhou B, Iannacchione GS, Garland CW, Bellini T. Random-field effects on the nematic-smectic-A phase transition due to silica aerosil particles. Phys. Rev. E. 1997;559(3):2962–2968.
[48] Wu L, Zhou B, Garland CW, Bellini T, Schaefer DW. Heat-capacity study of nematic-isotropic and nematic-smectic-A transitions for octylcyanobiphenyl in silica aerogels. Phys Rev E. 1995;51(3):2157.